Available online at www.sciencedirect.com
ScienceDirect
Journal of Crystal Growth 297 (2006) 146–151
JOURNAL OF CRYSTAL GROWTH
www.elsevier.com/locate/jcrysgro

Surface defects and mechanical hardness of rapidly grown DAST crystals

A.S. Haja Hameed[a], S. Rohani[a], W.C. Yu[b], C.Y. Tai[c], C.W. Lan[c,*]

[a]Department of Chemical and Biochemical Engineering, The University of Western Ontario, London, Ont., Canada N6A 5B9
[b]Department of Molecular Science and Engineering, National Taipei University of Technology, Taipei 106 Taiwan
[c]Department of Chemical Engineering, National Taiwan University, Taipei 10617, Taiwan

Received 29 August 2006; received in revised form 11 September 2006; accepted 25 September 2006
Communicated by K. Nakajima

Abstract

DAST crystals were grown by the two-zone growth technique and the crystal surfaces were analyzed with help of optical and scanning electron microscopic results. Owing to a high supersaturation in the growth zone, growth striations were observed on the {0 0 1} smooth surfaces (vicinal), while macrosteps were observed on the $\{0\,0\,\bar{1}\}$ rough surfaces of the grown crystals. Hillocks occurred on the F-surface, because new layers nucleated before the lateral growth of the deeper layers were completed. The microhardness of the grown crystals was measured on the (0 0 1) and (1 1 0) faces under different loads.

PACS: 42.70.Mp; 81.10.−Dn; 68.37.Ef; 62.20.−*x*

Keywords: A1. Convection; A1. Defects; A1. Optical microscopy; A1. Surfaces; A2. Growth from solution; B1. Organic compounds; B2. Nonlinear optical materials

1. Introduction

To realize the full use of nonlinear optical (NLO) crystals, efforts are required from crystal growth engineers to optimize crystal growth conditions. In general, the growth of large organic crystals is a difficult task because of the narrow metastable zones and hence the instability of the supersaturated solutions [1]. As the fabrication of devices often needs large crystals (several centimeter cube), the growth of crystals thus becomes a limiting step. Among a variety of NLO crystals, the organic ionic salt crystal 4-*N*, *N*-dimethylamino-4′-*N*-methyl-stilbazolium tosylate (DAST) is a very promising NLO material, which has been demonstrated to have a very large NLO susceptibility and the largest electro-optic (EO) coefficient of all materials researched to date [2–7]. Bulk single crystals of DAST are usually grown from a seeded saturated solution by the traditional slow cooling technique. It is also difficult to obtain large crystals by the slow cooling method, because spontaneous nucleation often occurs. For these reasons, the development of new techniques that can accelerate crystal growth is highly desirable [8]. In the present work, the two-zone growth technique (TZGT), which consists of a cold and a hot zone, was used to achieve high growth rates of DAST crystals by removing spontaneously nucleated crystals [9]. DAST crystals up to $32 \times 30 \times 8\,\mathrm{mm}^3$ in dimension were obtained in 17 days by the TZGT with a growth rate of 1.7 mm per day. The rapidly growing, faceted large crystals by TZGT also provided a unique chance to observe the surface morphology on certain faces. Furthermore, the high supersaturation in the growth zone allowed us to consider the existence of growth from edges and two-dimensional nucleation, and their connection with the defect formation process.

The present report focuses on the surface study of the grown crystals. To find out the surface features of the grown DAST crystals, an optical microscope and a

*Corresponding author. Tel./fax: +886 2 2363 3917.
E-mail address: cwlan@ntu.edu.tw (C.W. Lan).

0022-0248/$ - see front matter © 2006 Elsevier B.V. All rights reserved.
doi:10.1016/j.jcrysgro.2006.09.034

scanning electron microscope were used. Growth striations and macrosteps on the surfaces of the grown DAST crystals were described in detail. Microhardness of the rapidly grown crystals was also determined to assess the perfection of the crystals obtained at different temperature differences between the hot and cold zones.

2. Experimental procedure

DAST was synthesized by the condensation of 4-methyl-*N*-methyl pyridinium tosylate and 4-*N*, *N*-dimethylamino-benzaldehyde in the presence of piperidine [10,11]. The resulting DAST material was further purified by recrystallization from methanol. DAST crystals were grown from saturated methanol solutions by the TZGT [9]. In the present work, DAST crystals up to $32 \times 30 \times 8\,mm^3$ in dimension were grown by this technique for the first time.

The surfaces of the grown DAST crystals were examined with an optical (Model: OLYMPUS BX51) and a scanning electron (Model: SEM; HITACHI S-800) microscopes. SEM studies were conducted on the platinum coated (0 0 1) and (0 0 $\bar{1}$) faces of the crystals. Grown crystals of suitable sizes were used for microhardness measurements at room temperature using a Vickers microhardness tester (MODEL: HMV-2, Shimadzu, Japan). The {0 0 1} and {1 1 0} faces with smooth surfaces were selected for this study. Loads ranging from 10 to 100 g were used for indentation, while the indentation time was kept at 5 s for all cases. The impression of the indentation mark was square, and at least five indentations were made on each sample for each load. The diagonal length of each indentation was measured using a microscope equipped with a calibrated micrometer.

3. Results and discussion

In the TZGT, the temperature difference (ΔT) between the cold and the hot zones creates a concentration and temperature gradient between the growth and the nutrient cells. Through a combination of diffusion and thermal convection, the solute is transported from the nutrient to the growth cell, and the transport rate increases with increasing ΔT. From a previous study [9], a large ΔT led to a high growth rate, but crystal quality slightly deteriorated. Fig. 1 shows the DAST crystal grown at $\Delta T = 10\,^{\circ}C$ and the deviation between the crystal axis *a* and molecular axis *z* in DAST crystal. In the crystal structure of DAST [12], the anionic tosylate serves to line up adjacent rows of cationic chromophores in a parallel manner leading to an excellent alignment of chromophores within the crystal. X-ray studies of DAST crystals revealed that the large face of the plate contains the *ab* plane of the crystal structure with *a*- and *b*-axis along the diagonals. The only deviation from the completely aligned system is the 20° angle between the long axis of the molecule and the polar *a*-axis of the crystal as shown in Fig. 1. DAST crystal grows faster along *a*- and *b*-axis than the *c*-axis since {1 1 0} faces promote the growth rate of DAST crystals along the *a*- and *b*-axis.

The surfaces of the grown crystals were examined with both optical and scanning electronic microscopes. Microscopic studies of the grown crystals revealed a slightly fluctuated supersaturation near the growth faces of the DAST crystals. As per as the growth defects concerned, the growth layers were commonly observed on crystals grown from solution under relatively high supersaturation [14–18]. Sangwal et al. [15,17] reported the relation between growth kinetics and step bunching for L-arginine phosphate (LAP) crystals growing at various supersaturations.

As shown in Fig. 2, striations were formed on the (0 0 1) face at a high ΔT (10 °C), indicating a high supersaturation. At low growth rates, they are the dislocation sites, which are typically near the centers of the faces of growing DAST crystal. At high growth rates, the two-dimensional nucleation at corners predominates, so that step generation occurs primarily wherever the supersaturation is the greatest. However, such striations did not occur on the {0 1 2} and the {1 1 0} faces, although all faces were growing simultaneously. To maintain an efficient growth of DAST single crystals by the TZGT, it is essential to maintain an adequate material transport rate toward the growth interface. Too high material transport rate leads to a rise in supersaturation near the growing crystal, which in turn causes an increased rate of two-dimensional nucleation. Fig. 3 shows a schematic diagram to explain the existence of hillocks observed on the flat *F* surface of the crystal. It was assumed that several two-dimensional nuclei existed simultaneously, then new layers nucleated before

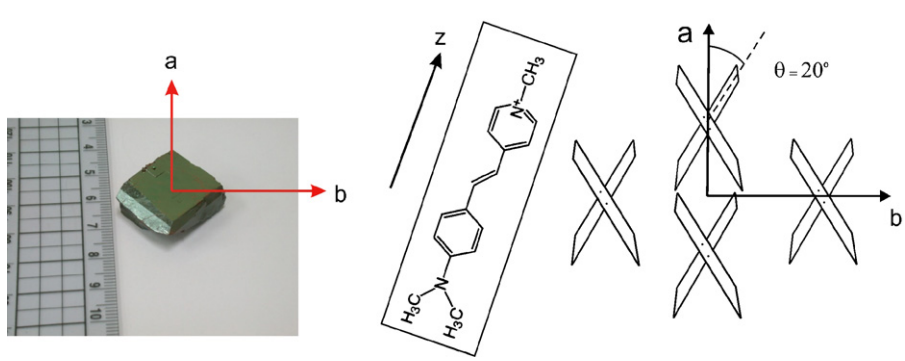

Fig. 1. DAST crystal ($32 \times 30 \times 8\,mm^3$) growth by the two-zone growth technique at $\Delta T = 10\,^{\circ}C$ for 17 days and the deviation between the crystal axis *a* and molecular axis *z* in DAST crystal.

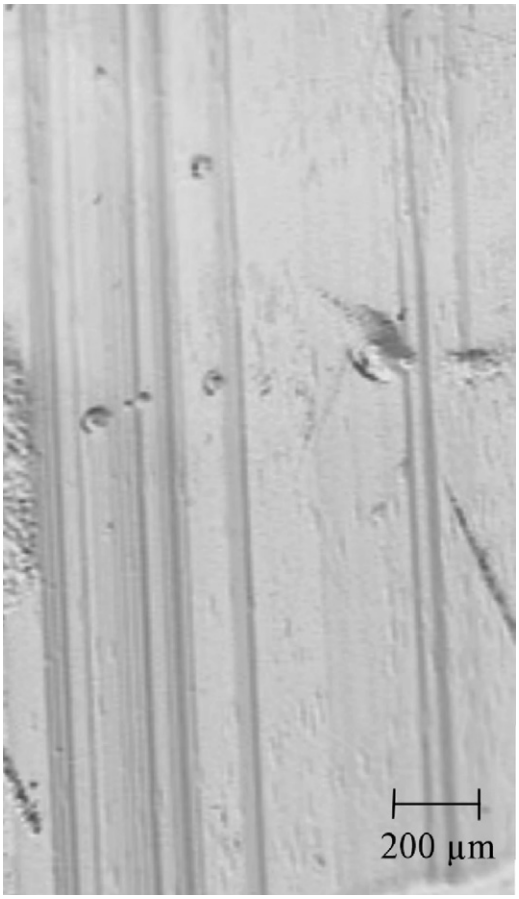

Fig. 2. Striations on the (0 0 1) face of the DAST crystal grown at $\Delta T = 10\,^{\circ}\mathrm{C}$.

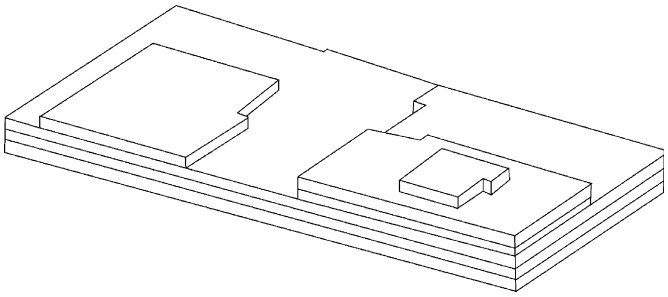

Fig. 3. Schematic diagram to illustrate two-dimensional nucleation.

lateral growth of the previous layer were completed and hence the hillocks were developed on the former flat *F* surface. To understand this type of surface morphology with the molecular arrangement of DAST, the projection of two unit cells along the crystallographic *a*-, *b*-, and *c*-axis was helpful. Owing to high solute transfer, the fluctuation in growth rate makes irregular stacking of the chromophores and the tosylates leading to the surface defects like hillocks. Normally, the sheets of cationic chromophores are interleaved with sheets of *p*-toluene sulfonate (tosylate) anions along the crystallographic *c*-axis. If it does not happen during the growth at faster rate, there is a serious problem to get defect-free crystals. We can understand the

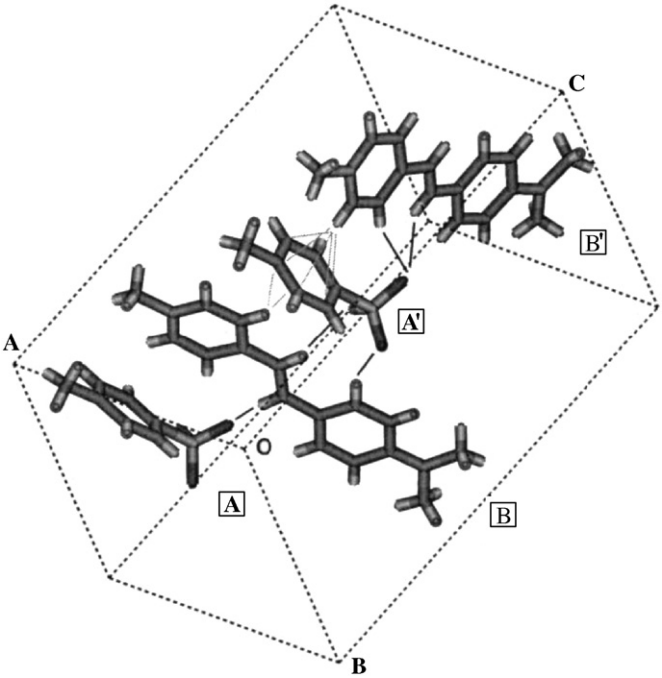

Fig. 4. Main interactions between anions and cations along the *c* axis. Notice the *A*-*B*-*A*′-*B*′ packing of the alternate chromophores and tosylates. As a result of the tilt angle, 20°, binding interactions are different in the *A*–*B* and the *A*′–*B*′ sheets. Darker lines, shortest tosylate–stilbazolium bindings; lighter lines, weaker interactions. For clarity, only half of the chromophores are displayed [13].

interleaving of the sheets of both ions (chromophore and tosylate) from Fig. 4, in which the pattern formed by the successive sheets is of the form *A*–*B*–*A*′–*B*′–*A*–*B*–*A*′–*B*′– …, with *A* and *A*′ representing the two nonequivalent anions and *B* and *B*′ the two nonequivalent cations [13]. From the above statement, we can understand that the orientation of the cationic chromophore and anionic tosylate in the DAST crystal lattice with respect to its dielectric axes plays an important role while growing DAST crystals at high growth rate.

Fig. 5 shows the SEM photograph for the formation of hillocks on the flat surface of the DAST crystal. On the surface, the cation–anion interactions occur perpendicularly to the interleaved sheets of anions and cations, i.e., along the *c*-axis. Moreover, mother liquid droplets trap between these hillocks and overgrow in the further crystallization process. The tendency of inclusions increases with increasing growth rate and crystal size. Both of these parameters depend on the supersaturation around the crystal face. The fluctuations of growth rate can also significantly increase inclusion formation.

In addition, uniform step-trains on crystal surfaces growing under diffusion-limited conditions are subject to several hydrodynamic/diffusion-based instability mechanisms [19]. Fig. 6(a) shows dense macrosteps on the $(0\,0\,\bar{1})$ near the seed and away from the seed. The reduced solution concentration at the leading edge slowed down the steps relative to those at the back of the step train, because there was less material at the leading edge available for

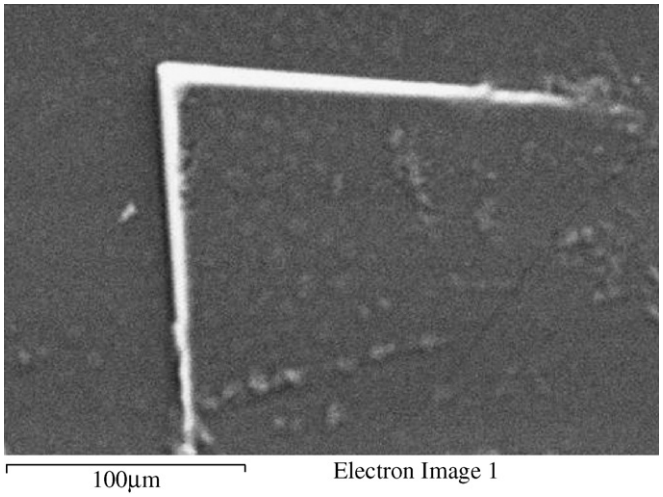

Fig. 5. SEM photograph for the formation of hillocks on the flat surface of DAST crystal.

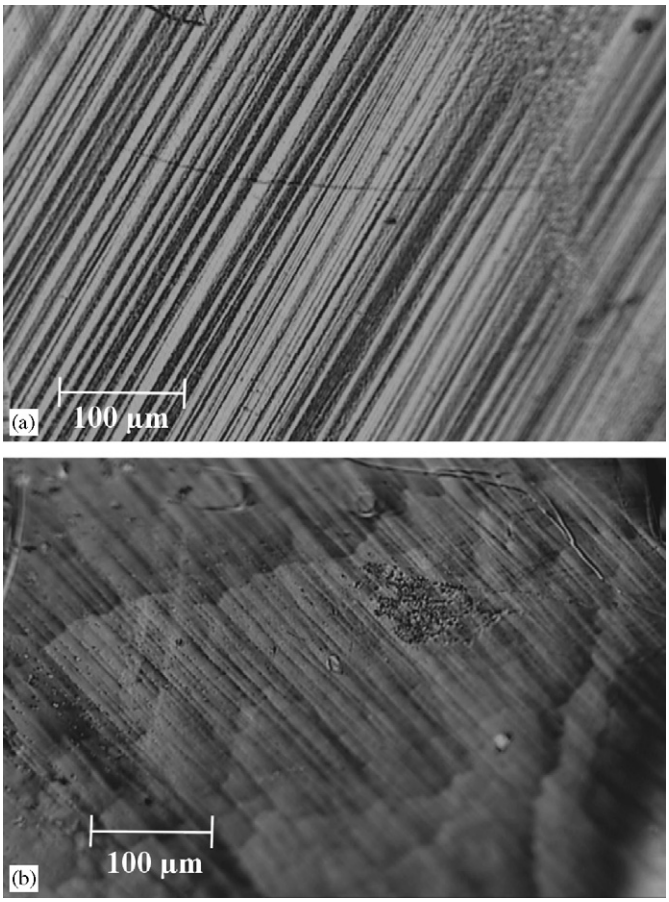

Fig. 6. Densely formed macrosteps on the $(0\,0\,\bar{1})$: (a) near the seed and (b) away from the seed.

incorporation into the crystal surface. Fig. 6a shows the photograph of a small region located near the bottom of the face, which was covered by the crowded macrosteps. This region of the face was unstable. The pronounced nonuniformity of step propagation observed on this face was due to the fluctuation of surface supersaturation. The

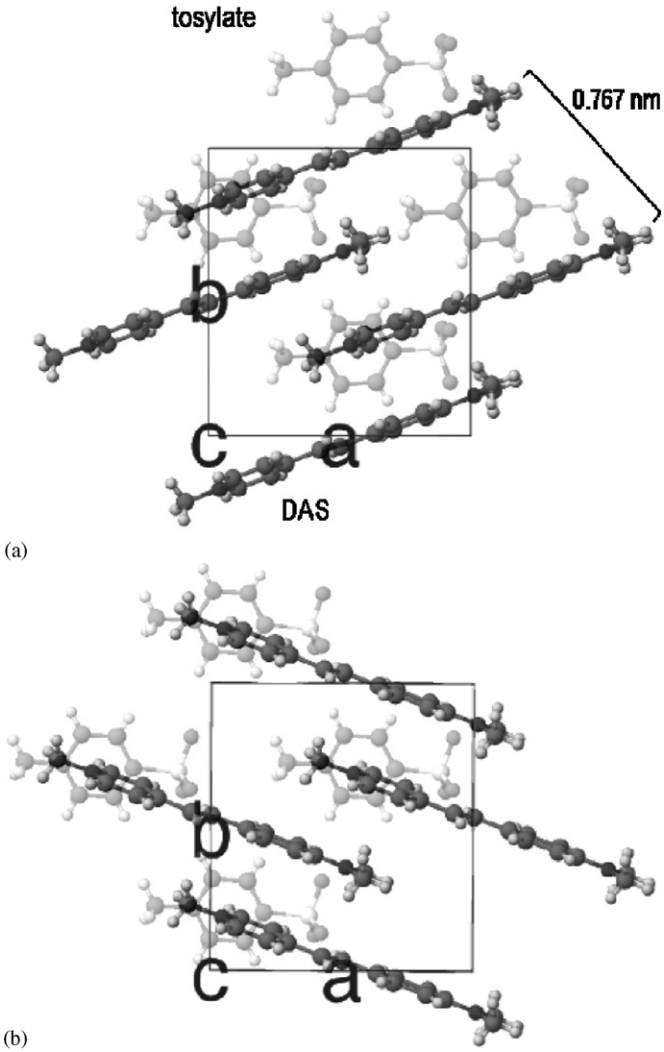

Fig. 7. Molecular arrangement of the DAST *ab*-plane: (a) one-pair layer, (b) the next-pair layer. The darker molecules are DAS (cation), and the lighter molecules are tosylate (anion) [20].

contour lines bended as they traveled up to the top of the crystal. This occurred because the surface supersaturation was higher near the edges of the face than at the center. In the region just below the seeded area, the same contour lines (Fig. 6b) propagated along the bottom edge of the face. The photograph shows that macrosteps propagated from the lower right edge to the lower left corner. No macrosteps were seen at the top of the crystal. The macrosteps are parallel to the *ab* plane of the DAST crystals in which a one-pair layer and the next-pair layer of DAST molecules (the planar chromophore (DAS)) are located perpendicularly to the $\{0\,0\,1\}$. This type of the molecular arrangement of the DAST is shown in Fig. 7 [20].

Closer to the seeded area, some protrusions of clusters were found, due to the presence of strains and surface roughness resulted from the rapid growth (Fig. 8(a)). Some aggregations of clusters accumulated near the seeded area because of the gluing the seed crystal to the Teflon strip.

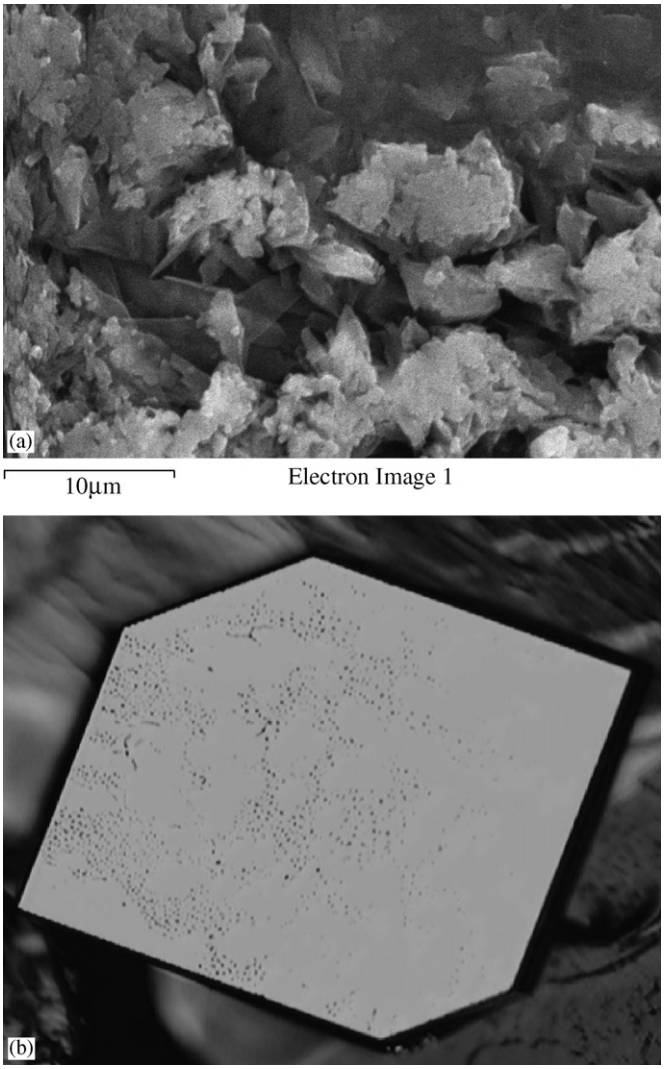

Fig. 8. (a) Protrusions of clusters due to the presence of strains and surface roughness. (b) Microcrystal observed on (0 0 $\bar{1}$) face of the grown crystal.

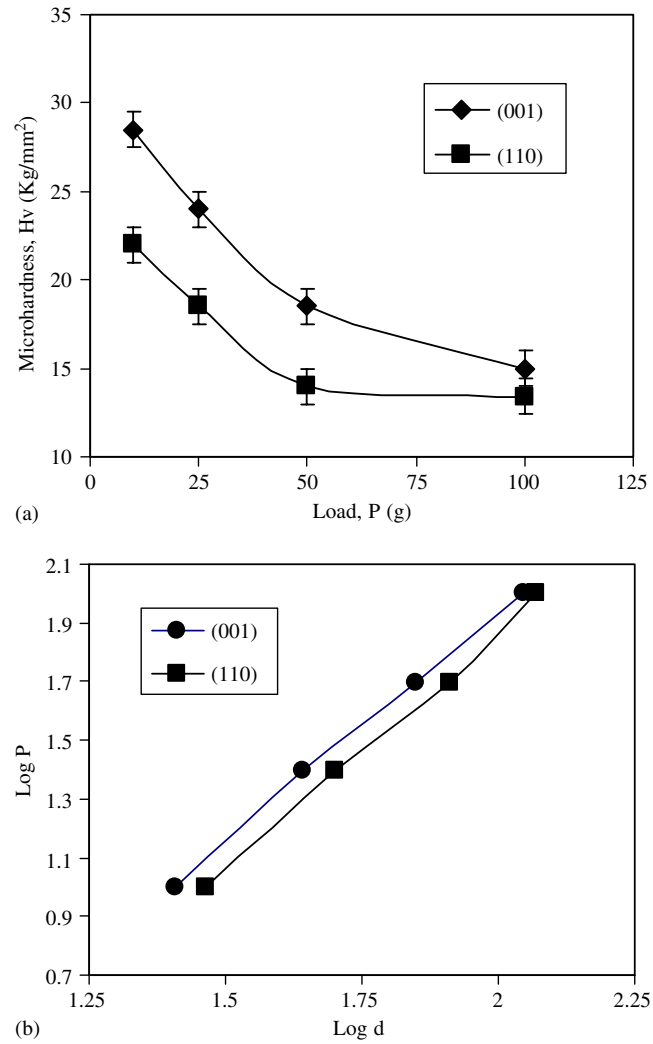

Fig. 9. (a) Microhardness number (H_v) versus load (P) curves on (0 0 1) and (1 1 0) faces of DAST crystal. (b) Log P versus log d curves on (0 0 1) and (1 1 0) faces of DAST crystal.

Mechanical stress was induced on the (0 0 $\bar{1}$) due to the gluing. Owing to the formation of macrosteps as discussed in the previous section and micro crystals on (0 0 $\bar{1}$) face of DAST crystals, the surface of the face was not smoothly developed. One of the micro crystals observed on the (0 0 $\bar{1}$) of the DAST crystals is shown in Fig. 8(b). Even in the micro crystal, the (0 0 $\bar{1}$) face was found to be microscopically rough. So, after a prolonged growth, the (0 0 $\bar{1}$) face of DAST crystal became rougher.

Even though DAST crystals have no cleavage planes, the cutting and polishing of the bulk crystals are done with less difficulty along the {0 0 1} planes. So, the hardness on (0 0 1) face is quite important for material processing. The hardness studies were done on (0 0 1) and (1 1 0) faces of the grown DAST crystals. Owing to the formation of macro steps and micro crystals on (0 0 $\bar{1}$) face of DAST crystals, it was difficult to proceed the indentation experiments on this face. In this experiment, the average diagonal length of the indented impression was calculated, and the Vickers microhardness number (H_v) was found from the relation of $H_v = 2P\sin(\theta/2)/d^2$. If the P is the applied load (in kg) and d is the average diagonal length of the indentation impressions (mm), and the angle between the opposite faces of the diamond pyramid is $\theta = 136°$, then H_v in kg/mm^2 is given by

$$H_v = 1.8544\, P/d^2. \quad (1)$$

The variation of microhardness (H_v) with applied load for the faces (0 0 1) and (1 1 0) showed that with the increase of applied load, the hardness number decreased in an asymptotic manner, reaching a saturation value at higher load (Fig. 9a). This was due to the fact that energy associated with the indenter was low at lower load (10 g), so that dislocation at the point of indentation did not allow the indenter to penetrate further. On the other hand, at higher load the indenter could easily penetrate owing to the movement of dislocations away from the indenter. Therefore, the hardness number decreased rapidly and was not

affected with further increase in the load. The hardness number observed on (0 0 1) was higher than that of (1 1 0) and this might be due to the more hardened lattice in (0 0 1). Onitsch [21] reported in Kick's correlation ($P = Kd^n$) that if the value of work hardening coefficient n is less than or equal to 2, the microhardness number decreases with the increase of load. The slope of the log d versus log P curves (Fig. 9b) for the two planes gives the n values of 1.55 for (0 0 1) plane and 1.61 for (1 1 0) plane of the crystal. This result clearly agrees with the report of Onitsch. The nonlinear variation of microhardness may be due to the presence of imperfections, which were observed during the surface analysis of the DAST crystals and the orientation of chromophores. The variation of microhardness on the {0 0 1} and {1 1 0} planes is due to the interaction of cations and anions associated with the DAST molecular structure. The relatively strong interaction between the cationic and anionic planes or strong ionic bond between anion–cation pairs is responsible for the mechanical strength of DAST crystals. Comparatively high cohesive energy of DAST along the c-axis provided by the tosylate–chromophore interactions causes for the difference in hardness values on (0 0 1); it coincides with the close packing of atoms in the plane, compared to (1 1 0) that has loosely packed lattice due to the reduced bond energy and hence it has a reduced hardness value. From our investigation, it is clear that there is considerable anisotropy in the mechanical hardness of DAST crystal. This again must be due to the highly anisotropic nature of the bonding environment in the crystal.

4. Conclusions

Growth striations were observed due to high-temperature gradient in the growth zone. Owing to the concurrent existence of several two-dimensional nuclei and bunching effects during the growth, further layers nucleated before lateral growth were completed and the former flat F surface developed hillocks. The nonuniform propagation of macrosteps was pronounced on the $(0\,0\,\bar{1})$. The dependence of microhardness on loads was found on the (0 0 1) and (1 1 0) faces. In connection with the molecular structure of DAST, surface morphology of the grown DAST crystals was explained. The decrease of microhardness with the increase of load was observed. The work hardening coefficients for (0 0 1) and (1 1 0) faces agreed well with Onitch's report [21].

References

[1] H.E. Buckley, Crystal Growth, Wiley, New York, 1951.
[2] S.R. Marder, J.W. Perry, W.P. Schaefer, Science 245 (1989) 626.
[3] C.P. Yakymyshyn, K.R. Stewart, E.P. Boden, S.R. Marder, J.W. Perry, P. Schaefer, in: Proceedings of the Second International Symposium on Organic Materials for Non-linear Optics, Royal Society of Chemistry, Cambridge, UK, 1991, p. 108.
[4] G. Knofple, R. Schlesser, R. Ducret, P. Gunter, Nonlinear Opt. 9 (1995) 143.
[5] F. Pan, G. Knofple, Ch. Bosshard, S. Follonier, R. Spreiter, M.S. Wong, P. Gunter, Appl. Phys. Lett. 69 (1996) 13.
[6] C. Bosshard, R. Spreiter, P. Gunter, J. Opt. Soc. Am. B 18 (2001) 1620.
[7] K. Nagaoka, H. Adachi, S. Brahadeeswaran, T. Higo, M. Takagi, M. Yoshimura, Y. Mori, T. Sasaki, Jpn. J. Appl. Phys. 43 (2004) L261.
[8] N.P. Zaitseva, J.J. De Yoreo, M.R. Dehaven, R.L. Vital, K.E. Montgomery, M. Richardson, L.J. Atherton, J. Cryst. Growth 180 (1997) 255.
[9] A.S. Haja Hameed, W.C. Yu, Z.B. Chen, C.Y. Tai, C.W. Lan, J. Crystal Growth 282 (2005) 117.
[10] H. Adachi, Y. Takahashi, J. Yabuzaki, Y. Mori, T. Sasaki, J. Crystal Growth 198–199 (1999) 568.
[11] J.I. Wu, R. Gopalakrishnan, C.I.D. Tai, C.W. Lan, Jpn. J. Appl. Phys. 43 (2004) 1507.
[12] S.R. Marder, J.W Perry, C.P. Yakymyshyd, Chem. Mater. 6 (1994) 1137.
[13] S. Follonier, M. Fierz, I. Biaggio, U. Meier, Ch. Bosshard, P. Gunter, J. Opt. Soc. Am. 19 (2002) 1990.
[14] M. Rak, K. Sangwal, J. Crystal Growth 65 (1983) 494.
[15] K. Sangwal, J. Torrent-Burgers, F. Sanz, P. Gorostiza, J. Crystal Growth 172 (1997) 209.
[16] K. Sangwal, M. Szurgot, J. Crystal Growth 79 (1986) 829.
[17] K. Sangwal, S. Veintemillas-Verdaguer, J. Torrent-Burgers, J. Crystal Growth 155 (1995) 135.
[18] A.J. Derksen, W.J.P. Van Enckevort, M.S. Couto, J. Appl. Phys. D 27 (1994) 2580.
[19] W.A. Tiller, The Science of Crystallization: Macroscopic Phenomena and Defect Generation, Cambridge University Press, Cambridge, New York, Port Chester, Melbourne, Sydney, 1991, p. 8f.
[20] H. Nanjo, P. Qian, N. Sanada, T.M. Suzuki, H. Takahashi, H. Ito, K. Komatsu, Opt. Lett. 25 (2000) 1107.
[21] E.M. Onitsch, Mikroskopie 95 (1956) 12.